INTERNATIONAL JOURNAL FOR NUMERICAL METHODS IN FLUIDS
Int. J. Numer. Meth. Fluids 2009; **60**:1055–1078
Published online 20 October 2008 in Wiley InterScience (www.interscience.wiley.com). DOI: 10.1002/fld.1897

Collocated discrete least squares meshless (CDLSM) method for the solution of transient and steady-state hyperbolic problems

M. H. Afshar*, †, ‡, M. Lashckarbolok and G. Shobeyri

Civil Engineering Faculty, Iran University of Science and Technology, Iran

SUMMARY

A collocated discrete least squares meshless method for the solution of the transient and steady-state hyperbolic problems is presented in this paper. The method is based on minimizing the sum of the squared residuals of the governing differential equation at some points chosen in the problem domain as collocation points. The collocation points are generally different from nodal points, which are used to discretize the problem domain. A moving least squares method is employed to construct the shape functions at nodal points. The coefficient matrix is symmetric and positive definite even for non-symmetric hyperbolic differential equations and can be solved efficiently with iterative methods. The proposed method is a truly meshless method and does not require numerical integration. Advantages of the collocation points are shown to be threefold: First, the collocation points are shown to be responsible for stabilizing the method in particular when problems with shocked solution are attempted. Second, the collocation points are also shown to improve the accuracy of the solution even for problems with smooth solutions. Third, the collocation points are shown to contribute to the efficiency of the method when solving steady-state problems via faster convergence of the resulting algorithm. The ability of the method and in particular the effect of collocation points are tested against a series of one-dimensional transient and steady-state benchmark examples from the literature and the results are presented. A sensitivity analysis is also carried out to investigate the effect of the base polynomials on the accuracy and convergence characteristics of the method in solving steady-state problems. The results show the ability of the proposed method to accurately solve difficult hyperbolic problems considered. The method is also shown to be particularly stable for problems with shocked solution due to the inherent stabilizing mechanism of the method. Copyright © 2008 John Wiley & Sons, Ltd.

Received 19 November 2007; Revised 24 May 2008; Accepted 13 July 2008

KEY WORDS: meshless method; collocated discrete least squares; transient; steady state; hyperbolic problems

*Correspondence to: M. H. Afshar, Civil Engineering Faculty, Iran University of Science and Technology, Iran.
†E-mail: mhafshar@iust.ac.ir
‡Associate Professor.

1. INTRODUCTION

The use of a mesh is a basic characteristic of traditional numerical approaches for the solution of partial differential equations. In those approaches, assumptions are made for the local approximation of the unknown variables, which require a mesh to support them. Generation of appropriate meshes, however, is a difficult and time-consuming task especially in problems with moving boundaries.

During recent years, considerable effort has been given to the development of so-called meshfree (meshless) methods. The aim of this type of approach is to eliminate at least the structure of the mesh and approximate the solution entirely using values at nodes arbitrarily distributed inside the domain and/or on the boundary. Many meshless (or particle) methods have been reported in the past decade, such as element free Galerkin [1], diffusive element method (DEM) [2], reproducing kernel particle (RKPM) [3], smoothed particle hydrodynamics (SPH) [4, 5], moving particle semi-implicit (MPS) [6], partition of unity (PU) [7], and meshless local Petrov–Galerkin (MLPG) [8].

According to using or not requiring integration, meshless methods can be largely grouped into two different categories: meshless methods based on strong forms of the governing differential equations and meshless methods based on weak forms of the governing differential equations. The meshless methods based on the strong forms have a long history of development. One widely used is the meshless collocation method, in which the strong forms of the governing differential equations are directly collocated in the selected collocation points. In the paper of Onate *et al.* [9], a procedure called finite point method (FPM) was proposed using a normal weighted least squares interpolation with the use of a fixed Gaussian weight functions. The governing differential equations were discretized into a non-integral type of the discrete equation system using a point collocation technique. The method that could be interpreted as a generalized form of the finite difference methods was successfully applied to the problems of convective diffusive transport. The meshless collocation methods has the following attractive advantages: (1) it is very easy to be coded and simple to be implemented; (2) it is computationally efficient because no numerical integration is required; and (3) it is a truly meshless method not requiring any mesh for both field variable approximation and integration. Owing to the above advantages, the meshless collocation methods have been widely used in computational mechanics. However, the meshless collocation method also has some shortcomings. (1) It is often unstable and less accurate. This is because in the collocation method, the governing equations and its boundary conditions are only considered on the collocation points, whereas they are neglected on the other points. (2) It is difficult to enforce boundary condition, especially the derivative (Neumann) boundary conditions. The Neumann boundary conditions are usually enforced using a series of separate equations resulting in instability of the solution. (3) The final coefficient matrix is usually asymmetric.

To overcome the above shortcomings of the meshless collocation method, some modified collocation methods have been developed. Zhang *et al.* [10] developed the least squares collocation method for the solution of elliptic problems. In this method, a set of over determined system of equations, in which the number of equations is greater than the unknowns, was constructed and the least squares technique was used to solve it. Liu *et al.* [11] proposed a meshless weighted least squares (MWLS) method to solve steady and unsteady heat conduction problems. A Hermite-type collocation method was also suggested by Liu *et al.* [12] to consider both governing equations and boundary conditions on Neumann boundaries. Xiaofei *et al.* [13] carried out a sensitivity analysis on the MWLS parameters for solving the problems of a cantilever beam and an infinite plate with a central circular hole. Error estimates for moving least squares (MLS) approximations in the one-dimensional case of convection–diffusion problems were investigated by

DOI: 10.1002/fld

Armentano and Durán [14]. A point weighted least squares method was developed by Wang *et al.* [15] and tested on one- and two-dimensional Poisson equations. Afshar and Arzani [16] developed discrete least squares meshless (DLSM) method for the solution of elliptic problems on uniform mesh of nodes. In this method a fully least squares approach was used in both function approximation and discretization of the governing differential equations. This method is based on minimizing a least squares functional with respect to the nodal parameters. The least square functional is formed as the weighted squared residuals of the governing differential equations and its boundary conditions at nodal points. An improved version of DLSM has been recently proposed in which the least square functional is formed at the nodal points and some auxiliary points chosen on the problem domain and its boundaries. The method was shown to improve the performance of the method used to solve one- and two-dimensional elliptic problems on highly irregular mesh of nodes [17].

All the least-squares-based collocation methods proposed so far, however, have been used to solve only problems of elliptic nature. Neither of the least-squares-collocation-based methods introduced so far have been used to solve hyperbolic problems nor has any new method been introduced for this purpose.

In this paper a collocated discrete least squares meshless (CDLSM) method is presented for the solution of steady-state and transient hyperbolic problems. The method constructs the least squares functional as the weighted sum of squared residuals of the governing differential equations and its boundary conditions at some collocation points, which include the nodal points used to discretize the problem domain and its boundaries. The method does not require a numerical integration due to the discrete nature of the functional and, therefore, is a truly meshless method. The method has the additional advantage of producing symmetric, positive-definite matrices even for non-self-adjoint problem such as those encountered in the fluid flow problems. The method is used here to solve a series of one-dimensional transient and steady-state hyperbolic benchmark problems from the compressible and incompressible flow discipline and the results are presented. These experiments show that proposed CDLSM method is capable of producing stable and accurate results for difficult problems considered. The effect of the collocation points are also investigated on the stability, accuracy and convergence characteristics of the method and the results are presented.

2. MOVING LEAST SQUARES (MLS) METHOD

Different techniques have been proposed and used to construct shape functions in the development of the meshless methods. The MLS approximation by Lancaster and Salkauskas [18], the radial point interpolation method (RPIM) by Liu and Gu [19] and the Kriging interpolation by Gu [20] are only some examples of existing methods. Among these approximation methods the MLS method has been widely used for function approximation by meshless community. In MLS, the function to be approximated is represented by

$$u^h(\mathbf{x}) = \sum_{i=1}^{m} p_i(\mathbf{x}) a_i(\mathbf{x}) \equiv \mathbf{p}^{\mathrm{T}}(\mathbf{x})\mathbf{a}(\mathbf{x}) \tag{1}$$

Here $\mathbf{p}^{\mathrm{T}}(\mathbf{x})$ is a set of linearly independent polynomial basis and $\mathbf{a}(\mathbf{x})$ represents the unknown coefficients to be determined by the fitting algorithm. In MLS approximation, at each point $\mathbf{x}$, $\mathbf{a}(\mathbf{x})$

DOI: 10.1002/fld

is chosen to minimize the sum of weighted squared residuals defined as

$$J=\frac{1}{2}\sum_{I=1}^{n} w(|\mathbf{x}-\mathbf{x}_I|)[\mathbf{p}^{\mathrm{T}}(\mathbf{x}_I)\mathbf{a}(\mathbf{x})-u_I]^2 \tag{2}$$

where u_I is the nodal value of the function to be approximated, n is the number of nodes and $w(|\mathbf{x}-\mathbf{x}_I|)$ is the weight function defined to have compact support. Different weight functions have been proposed and used by different researchers. Ataie-Ashtiani and Farhadi [6] tested different weight functions for solving two-dimensional dam break problem concluding that a cubic kernel function considerably improves the stability and accuracy of the approximation. Here a one-dimensional cubic spline is used as the weight function, which is defined as

$$w(r)=\begin{cases} \frac{2}{3}-4r^2+4r^3 & \text{for } r\leqslant\frac{1}{2} \\ \frac{4}{3}-4r+4r^2-\frac{4}{3}r^3 & \text{for } \frac{1}{2}<r\leqslant 1 \\ 0 & \text{for } r>1 \end{cases} \tag{3}$$

where $r=s/s_{\max}$, $s=\|\mathbf{x}-\mathbf{x}_I\|$ and $s_{\max}$ is the radius of the support domain for each node. Equation (2) can be expressed in matrix form as

$$\mathbf{J}=(\mathbf{Pa}-\mathbf{u})^{\mathrm{T}}\mathbf{W}(\mathbf{Pa}-\mathbf{u}) \tag{4}$$

where

$$\mathbf{u}^{\mathrm{T}}=(u_1,u_2,\ldots,u_n) \tag{5}$$

$$\mathbf{P}=\begin{bmatrix} p_1(\mathbf{x}_1) & p_2(\mathbf{x}_1) & \cdots & p_m(\mathbf{x}_1) \\ p_1(\mathbf{x}_2) & p_2(\mathbf{x}_2) & \cdots & p_m(\mathbf{x}_2) \\ \vdots & \vdots & \vdots & \vdots \\ p_1(\mathbf{x}_n) & p_2(\mathbf{x}_n) & \cdots & p_m(\mathbf{x}_n) \end{bmatrix} \tag{6}$$

and

$$\mathbf{W}(\mathbf{x})=\begin{bmatrix} w(|\mathbf{x}-\mathbf{x}_1|) & 0 & \ldots & 0 \\ 0 & w(|\mathbf{x}-\mathbf{x}_2|) & \ldots & 0 \\ \vdots & \vdots & \vdots & \vdots \\ 0 & 0 & \ldots & w(|\mathbf{x}-\mathbf{x}_n|) \end{bmatrix} \tag{7}$$

The coefficients $\mathbf{a}(\mathbf{x})$ are found by minimizing $\mathbf{J}$ with respect to them. Carrying out the differentiation we may have

$$\frac{\partial \mathbf{J}}{\partial \mathbf{a}}=\mathbf{A}(\mathbf{x})\mathbf{a}(\mathbf{x})-\mathbf{B}(\mathbf{x})\mathbf{u}=0 \tag{8}$$

DOI: 10.1002/fld

where

$$\mathbf{A}=\mathbf{P}^{\mathrm{T}}\mathbf{W}(\mathbf{x})\mathbf{P} \tag{9}$$

$$\mathbf{B}=\mathbf{P}^{\mathrm{T}}\mathbf{W}(\mathbf{x}) \tag{10}$$

Solving the above equation for the unknown parameters $\mathbf{a}(\mathbf{x})$ results in

$$\mathbf{a}(\mathbf{x})=\mathbf{A}^{-1}(\mathbf{x})\mathbf{B}(\mathbf{x})\mathbf{u} \tag{11}$$

The approximation of the unknown function can now be expressed in a familiar form of

$$\mathbf{u}^h(\mathbf{x})=\sum_{i=1}^{n}\mathbf{N}_i(\mathbf{x})\mathbf{u}_i \tag{12}$$

where $\mathbf{N}_i(\mathbf{x})$ denotes the shape function of node i and can be obtained from the following relationship:

$$\mathbf{N}=\mathbf{p}^{\mathrm{T}}(\mathbf{x})\mathbf{A}^{-1}(\mathbf{x})\mathbf{B}(\mathbf{x}) \tag{13}$$

In this case, $\mathbf{u}_i \neq \mathbf{u}^h(x_i)$; hence, the parameters $\mathbf{u}_i$ cannot be treated like nodal values of the unknown function. The shape functions are not strict interpolants since they do not pass through the data. The shape functions do not satisfy the Kronecker delta condition:

$$N_i(\mathbf{x}_j)\neq\delta_{ij}=\begin{Bmatrix}1 & \text{if } i=j\\ 0 & \text{otherwise}\end{Bmatrix} \tag{14}$$

Here $N_i(\mathbf{x}_j)$ is the shape function of node i evaluated at node j and δ_{ij} is the Kronecker delta. Generally it is necessary to obtain the shape function derivatives. The first derivative of the shape functions are obtained as

$$\frac{\mathrm{d}\mathbf{N}(\mathbf{x})}{\mathrm{d}\mathbf{x}}=\frac{\mathrm{d}\mathbf{P}}{\mathrm{d}\mathbf{x}}\mathbf{A}^{-1}\mathbf{B}+\mathbf{P}\frac{\mathrm{d}(\mathbf{A}^{-1})}{\mathrm{d}\mathbf{x}}\mathbf{B}+\mathbf{P}\mathbf{A}^{-1}\frac{\mathrm{d}\mathbf{B}}{\mathrm{d}\mathbf{x}} \tag{15}$$

3. COLLOCATED DISCRETE LEAST SQUARES MESHLESS (CDLSM) METHOD

In this paper a time-marching method is used for the solution of steady-state hyperbolic problems so that a unified formulation can be used for both transient and steady-state cases. For this, consider the general form of differential equations governing the transient hyperbolic problems expressed in matrix form as

$$\frac{\partial\mathbf{u}}{\partial t}+\mathbf{A}(\mathbf{u})\frac{\partial\mathbf{u}}{\partial x}=\mathbf{Q}(\mathbf{u}) \quad \text{on } \Omega \tag{16}$$

subject to appropriate Dirichlet boundary condition:

$$u=\overline{\mathbf{u}} \quad \text{on } \Gamma_u \tag{17}$$

Here $\mathbf{u}$ denotes the problem unknown vector, $\mathbf{A}$ is the Jacobian matrix that is generally a function of the unknown vector $\mathbf{u}$ and $\mathbf{Q}$ is the source term.

DOI: 10.1002/fld

A semi-discretization is first carried out using the θ method in time:

$$\mathbf{u}^{n+1}-\mathbf{u}^n+\Delta t\theta\left[\mathbf{A}^{n+1}\frac{\partial \mathbf{u}^{n+1}}{\partial x}-\mathbf{S}^{n+1}\mathbf{u}^{n+1}\right]+\Delta t(1-\theta)\left[\mathbf{A}^n\frac{\partial \mathbf{u}^n}{\partial x}-\mathbf{Q}^n\right]=0 \tag{18}$$

with $\frac{1}{2}\leqslant\theta\leqslant 1$. Assuming $\mathbf{Q}=\mathbf{Su}$, the linearized residuals in the problem domain and its boundaries are now defined as

$$\mathbf{R}_\Omega=\mathbf{u}^{n+1}-\mathbf{u}^n+\Delta t\theta\left[\mathbf{A}^n\frac{\partial \mathbf{u}^{n+1}}{\partial x}-\mathbf{S}^n\mathbf{u}^{n+1}\right]+\Delta t(1-\theta)\left[\mathbf{A}^n\frac{\partial \mathbf{u}^n}{\partial x}-\mathbf{Q}^n\right]\neq 0 \quad \text{on } \Omega \tag{19}$$

$$\mathbf{R}_{\Gamma_u}=\mathbf{u}^{n+1}-\overline{\mathbf{u}} \quad \text{on } \Gamma_u \tag{20}$$

The domain residual can be expressed in a compact form as follows:

$$\mathbf{R}_\Omega=\mathbf{L}(\mathbf{u}^{n+1})+\mathbf{f} \quad \text{on } \Omega \tag{21}$$

where the differential operator $\mathbf{L}(\cdot)$ and term $\mathbf{f}$ are defined as

$$\mathbf{L}(\cdot)=(\cdot)+\Delta t\theta\left[\mathbf{A}^n\frac{\partial(\cdot)}{\partial x}-\mathbf{S}^n(\cdot)\right] \tag{22}$$

$$\mathbf{f}=-\mathbf{u}^n+\Delta t(1-\theta)\left[\mathbf{A}_j^n\frac{\partial \mathbf{u}^n}{\partial x_j}-\mathbf{Q}^n\right] \tag{23}$$

The philosophy of least squares is to find an approximate solution that minimizes the least squares functional to be defined later. For this, the problem domain and its boundaries are discretized by n nodal points. The approximate value of the function $\mathbf{u}$ at an arbitrary point x_k can be obtained through interpolation:

$$\mathbf{u}(x_k)=\sum_{i=1}^{n_k}N_i(x_k)\cdot\mathbf{u}_i \tag{24}$$

where n_k is the number of nodal points having x_k in their support domain.

The least squares functional is constructed as the sum of the weighted squared residuals of the differential equation and its boundary condition calculated at some points called collocation points chosen on the problem domain and its boundaries. Substituting Equation (24) into Equations (20) and (21) leads to the differential equation residual $\mathbf{R}_\Omega(x_k)$ and the Dirichlet boundary condition residual $\mathbf{R}_{\Gamma_u}(x_k)$ at a collocation point x_k defined as

$$\mathbf{R}_\Omega(x_k)=\mathbf{L}(\mathbf{u}^{n+1}(x_k))+\mathbf{f}(x_k) \quad \text{on } \Omega \tag{25}$$

$$\mathbf{R}_{\Gamma_u}(x_k)=\mathbf{u}^{n+1}(x_k)-\overline{\mathbf{u}}(x_k) \quad \text{on } \Gamma_u \tag{26}$$

Now the least squares functional defined as the weighted sum of the squared residuals at all collocation points can be constructed as

$$J=\frac{1}{2}\left(\sum_{k=1}^{M}[\mathbf{R}_\Omega(x_k)]^2+\alpha\cdot\sum_{k=1}^{M_u}[\mathbf{R}_{\Gamma_u}(x_k)]^2\right) \tag{27}$$

DOI: 10.1002/fld

where M is the total number of collocation points on the problem domain and its boundaries and M_u denotes the number of collocation points on the Dirichlet boundary. The factor α is the penalty parameter representing the relative weight of the boundary residuals with respect to the domain residuals. A large value of the penalty parameter is often used to ensure that the boundary conditions are accurately enforced.

Minimization of Equation (27) with respect to the nodal parameters $\mathbf{u}^{n+1}$ leads to

$$\frac{\partial \mathbf{J}}{\partial \mathbf{u}^{n+1}} = \sum_{k=1}^{M} \frac{\partial \mathbf{R}_\Omega}{\partial \mathbf{u}^{n+1}} [\mathbf{R}_\Omega] + \alpha \sum_{k=1}^{Mu} \frac{\partial \mathbf{R}_{\Gamma_u}}{\partial \mathbf{u}^{n+1}} [\mathbf{R}_{\Gamma_u}] = 0 \tag{28}$$

Substituting Equations (25) and (26) into Equation (28) yields the final system of equations:

$$\mathbf{K}\mathbf{U}^{n+1} = \mathbf{F} \tag{29}$$

where the typical components of matrix $\mathbf{K}$ and right-hand side vector $\mathbf{F}$ are defined as

$$K_{lm} = \sum_{i=1}^{Md} [\mathbf{L}(N_l)]_i^{\mathrm{T}} [\mathbf{L}(N_m)]_i + \alpha \sum_{i=1}^{Mu} [(N_l)]_i^{\mathrm{T}} [(N_m)]_i, \quad l, m = 1, \ldots, n \tag{30}$$

$$F_l = -\sum_{i=1}^{Md} [\mathbf{L}(N_l)]_i^{\mathrm{T}} \mathbf{f}_i + \alpha \sum_{i=1}^{Mu} [(N_l)]_i^{\mathrm{T}} (\overline{\mathbf{u}})_i, \quad l = 1, \ldots, n \tag{31}$$

The coefficient matrix $\mathbf{K}$ in Equation (30) can be seen to be symmetric and positive definite. Therefore, the final system of equations can be solved using efficient iterative procedure such as conjugate gradient methods if required. The system of equations can now be formed and solved to produce the required solution at each time step. For the steady-state problems, the solution is marched in time until a steady-state condition is reached. It should be noted here that the proposed time-marching method is stable for any time step sizes due to the implicit nature of the method. It can be seen that the proposed method is an extension of the DLSM method proposed by Afshar and Arzani [16] and Firoozjaee and Afshar [17] for the solution of elliptic problems. The method also has some in common with those methods used by Liu *et al.* [11] and Wang *et al.* [15] to solve problems of elliptic nature.

4. NUMERICAL EXAMPLES

The efficiency and accuracy of the proposed method to solve transient and steady-state hyperbolic problems is illustrated in this section by solving some one-dimensional transient and steady-state benchmark examples from the literature. A wide range of problems are considered to test the performance of the method in solving problems with shocked and smooth solutions. In the first section, the solution of some transient problems namely transient Burgers' equation, dam break problem and finally the shock tube problems are considered. The effects of time discretization and also collocation points on the stability and accuracy of the method to solve transient problems are also investigated. In the second section, the solution of steady Burgers' equation, steady flow over an ogee spillway and finally the nozzle problem under different boundary conditions are attempted. All the steady-state problems are solved using an Euler method defined by $\theta = 1$. The effect of the collocation methods and basis polynomial orders on the accuracy of the final solution and the convergence characteristics of the method are also investigated for steady-state problems.

DOI: 10.1002/fld

4.1. Formation and propagation of a discontinuity

This is a problem governed by the inviscid Burgers' equation defined by the following parameters of Equation (16):

$$\mathbf{A}=u, \quad \mathbf{Q}=0$$

The problem is solved on the domain $0\leqslant x\leqslant 1$ with the following initial and boundary conditions:

$$u(x,0)=2.0-5x, \quad 0\leqslant x\leqslant 0.2$$

$$u(x,0)=1.0, \quad 0.2\leqslant x\leqslant 1$$

$$u(0,t)=2.0, \quad x=0.0$$

Nodal spacing and time step sizes are chosen as $h=\Delta x=0.02$ and $\Delta t=0.01$. A polynomial basis of zero order ($P=[1]$) is used here. The shape functions are constructed through definition of $s_{\max}$ in a way that just three nodes are chosen in the local interpolation domain.

Some experiments are first carried out to examine the effect of θ and the number of collocation points on the solution. Figure 1 shows the results produced using $\theta=1$ and 51 collocation points coinciding with the nodal points. The results indicate that the solution of the problem with $\theta=1$ leads to smearing of the discontinuity as expected. It should be noted that the exact solution to this problem at times greater than $t=0.2$ is defined by a moving discontinuity with a velocity of 1.5 m/s. Figure 2 shows the results obtained using $\theta=0.5$ and the same number of collocation points as before. This value of θ was observed to lead to oscillatory solutions. This can be contributed to the fact that first-order time discretization of the governing equation defined by $\theta=1$ introduces larger implicit diffusion compared with second-order scheme defined by $\theta=0.5$, leading to more stable, though smoother, results already shown in Figure 1.

To overcome the difficulty of oscillatory results for the case of $\theta=0.5$, more collocation points are employed in construction of the least squares functional defined in Equation (27). Figure 3 shows the results obtained using $\theta=0.5$ and 501 uniformly distributed collocation points including

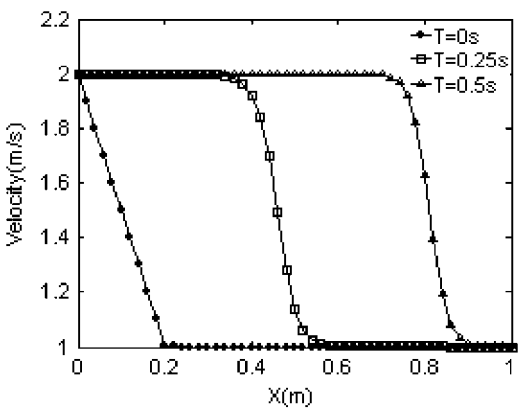

Figure 1. Formation and propagation of a discontinuity using $\theta=1$ and 51 collocation points.

DOI: 10.1002/fld

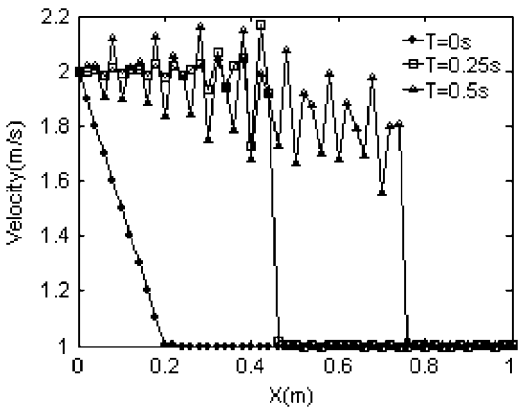

Figure 2. Formation and propagation of a discontinuity using $\theta=0.5$ and 51 collocation points.

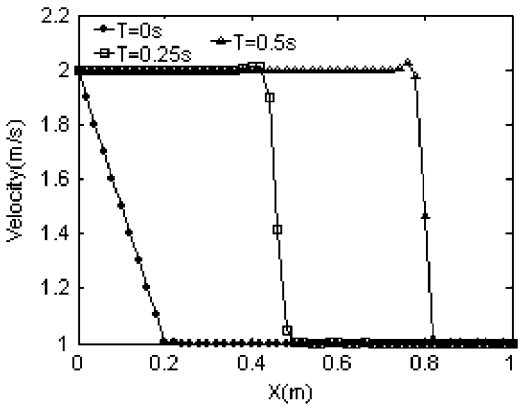

Figure 3. Formation and propagation of a discontinuity using $\theta=0.5$ and 501 collocation points.

51 nodal points illustrating significant improvement in the accuracy of the resulting solution. The shock is seen to be captured by just three nodal points with a very small overshoot.

4.2. Breaking of a dam

The non-linear shallow-water equations in one dimension governing the breaking of a dam can be defined with the following parameters of Equation (16):

$$\mathbf{u}=\begin{bmatrix} H+\eta \\ (H+\eta)u \end{bmatrix}, \quad \mathbf{A}=\begin{bmatrix} 0 & 1 \\ -u^2+g(H+\eta) & 2u \end{bmatrix}, \quad \mathbf{Q}=\begin{bmatrix} 0 \\ g(H+\eta)\dfrac{\mathrm{d}H}{\mathrm{d}x} \end{bmatrix}$$

where H is the depth, η is the surface elevation, u is the velocity, g is the acceleration due to gravity and $\mathrm{d}H/\mathrm{d}x$ is the bed slope. In the present study 81 nodes with uniform spacing was used to represent the problem domain in the range $0.0\,\mathrm{m}\leqslant x\leqslant 40\,\mathrm{m}$. The initial condition of $u=0$, $\eta=2$

DOI: 10.1002/fld

for $0\,\text{m} \leqslant x \leqslant 20\,\text{m}$ and $u=0$, $\eta=0$ for $20\,\text{m} < x \leqslant 40\,\text{m}$ was used. The depth H and g are assumed constant and equal to unity.

Figure 4 shows the water elevations obtained by the proposed method at $t=5\,\text{s}$ using $\theta=1$, $\Delta t=0.25\,\text{s}$, $\Delta x=0.5\,\text{m}$, 81 collocation points all coinciding with the nodal points, a polynomial basis of zero order ($P=[1]$) and $s_{\max}$ defined such that just three nodes are chosen in the local interpolation domain. The solution, though stable, is seen to be over-diffused due to the large implicit diffusion introduced by $\theta=1$. The problem was solved again using the same parameters as before except for the value of $\theta=0.5$ leading to oscillatory results shown in Figure 5 for water elevation. To overcome this difficulty another run was performed with 401 collocation points, 81 of which coinciding with the nodal points. Figure 6 shows the notable improvement in the accuracy of the solution by introducing more collocation points.

4.3. Shock tube problem

The shock tube problem is an example of one-dimensional compressible flow and governed by the one-dimensional Euler Equations:

$$\begin{bmatrix} \rho \\ \rho u \\ \rho e \end{bmatrix}_t + \begin{bmatrix} \rho u \\ \rho u^2 + P \\ \rho u H \end{bmatrix}_x = 0$$

Here, ρ is the density, u is the velocity, e is the specific total energy, P is the pressure, $H=\rho e+P$ is the total enthalpy and $\gamma=1.4$ is the ratio of specific heat. Pressure is related to other variables through the equation of state:

$$P=\rho(\gamma-1)(e-0.5u^2)$$

The governing equation can be defined in a quasi-linear form defined in Equation (16) with the following parameters:

$$\mathbf{u}=\begin{bmatrix} \rho \\ \rho u \\ \rho e \end{bmatrix}, \quad \mathbf{A}=\begin{bmatrix} 0 & 1 & 0 \\ -0.5(3-\gamma)u^2 & (3-\gamma)u & \gamma-1 \\ (\gamma-1)u^3-\gamma u e & \gamma e-1.5(\gamma-1)u^2 & \gamma u \end{bmatrix}$$

The initial condition of the problem is defined by a discontinuity at the center of the tube as follows:

$$\mathbf{u}=[1 \;\; 0 \;\; 2.5] \quad \text{for } x \leqslant 0.5$$

$$\mathbf{u}=[0.125 \;\; 0 \;\; 0.25] \quad \text{for } x > 0.5$$

A compression shock propagating into the low-pressure region is created after instantaneous removal of the discontinuity. In addition, the high pressure region hosts a propagating expansion wave. Figure 7 illustrates the solutions obtained at time $t=0.2\,\text{s}$ using the computational parameters of $\theta=1$, $\Delta t=0.005\,\text{s}$, $\Delta x=0.01\,\text{m}$ and 101 collocation points coinciding with the nodal points used to discretize the problem domain. Because of the implicit numerical diffusion introduced by using $\theta=1$, the compression wave is seen to be represented smoothly instead of a shock wave. To

DOI: 10.1002/fld

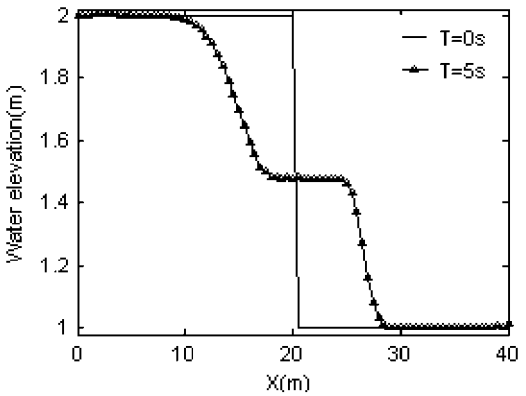

Figure 4. Water elevations obtained using $\theta = 1$ and 81 collocation points (dam break).

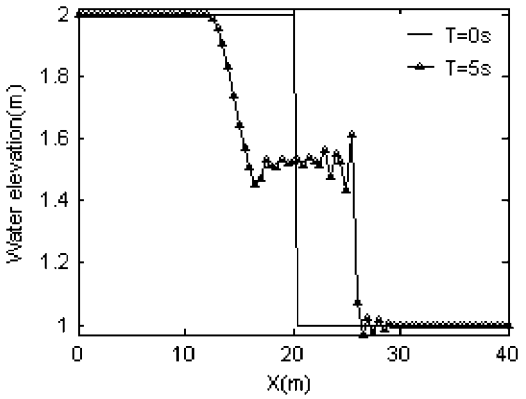

Figure 5. Water elevations obtained using $\theta = 0.5$ and 81 collocation points (dam break).

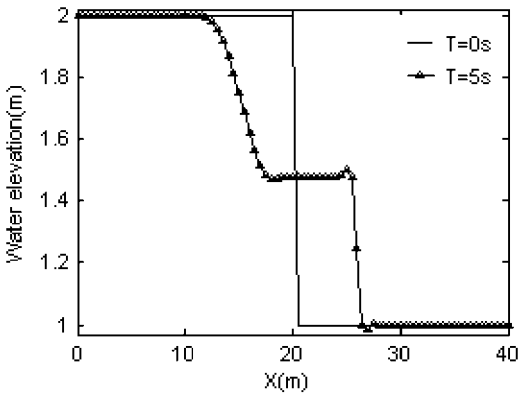

Figure 6. Water elevations obtained using $\theta = 0.5$ and 401 collocation points (dam break).

DOI: 10.1002/fld

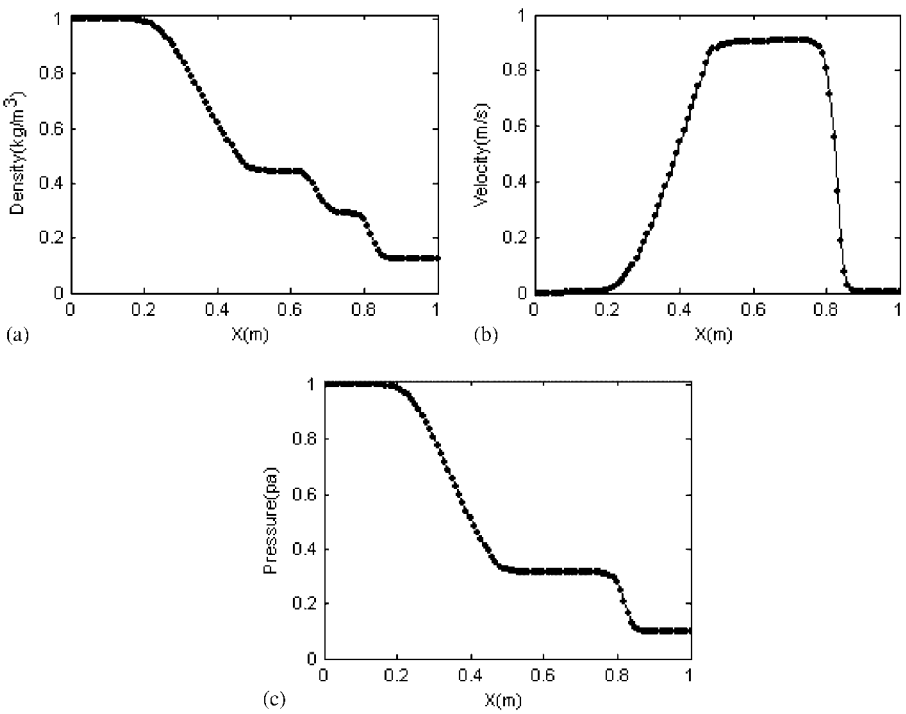

Figure 7. Variations of density (a), velocity (b) and pressure (c) obtained with $\theta=1$ and 101 collocation points (shock tube).

get more accurate results, a second run was performed using the same computational parameters as above except for $\theta=0.7$ leading to the results shown in Figure 8. The shock wave in all the variables is now represented more sharply compared with those of the first run but some oscillations are present around the shock wave, which is more evident for velocity. To overcome this difficulty, a third run was performed this time using 501 uniformly distributed collocation points, 101 of which coinciding with the nodal points. As seen from Figure 9, the oscillations nearly disappear while the sharpness of the shock wave in all three variables is preserved.

4.4. Steady Burgers' equation

This is a problem governed by the inviscid Burgers' equation defined by following parameters of Equation (16):

$$\mathbf{A}=u, \quad \mathbf{Q}=0$$

The problem was solved on the domain $0\leqslant x\leqslant 1$ with the following initial and boundary conditions:

$$u(x,0)=1.0-2x, \quad 0\leqslant x\leqslant 1$$

$$u(0,t)=1, \quad x=0.0$$

$$u(1,t)=-1, \quad x=1$$

DOI: 10.1002/fld

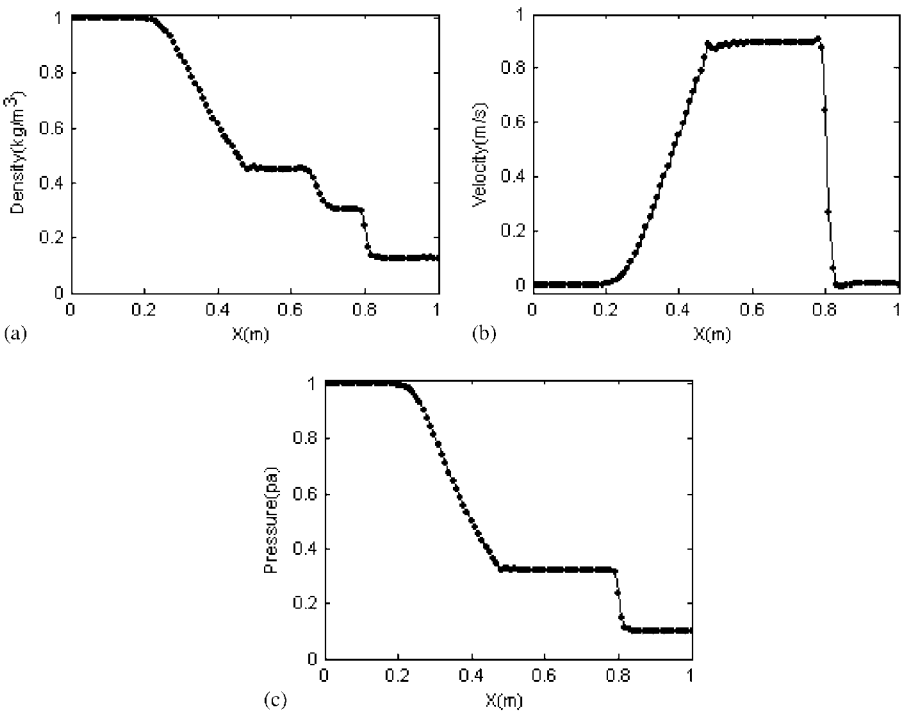

Figure 8. Variations of density (a), velocity (b) and pressure (c) obtained with $\theta = 0.7$ and 101 collocation points (shock tube).

The exact solution to this problem is represented by a discontinuity located at the center of the domain. The problem was solved here on a mesh of 51 equally distributed nodes using a time step size of 0.01. The solution of the problem is first attempted using 51 collocation points coinciding with the nodal points using different polynomial basis of order zero ($P = [1]$), one ($P = [1, x]$) and two ($P = [1, x, x^2]$). The radius of support domains used in each case was considered to be 0.027, 0.027, and 0.047, the minimum required to be able to construct the MLS shape functions. No converged solutions were obtained in these cases due to persistent oscillations at the shock position. The resulting un-converged solutions are shown in Figure 10 for different basis orders at time 1 s. As seen from the figure, oscillations are more prominent with higher-order polynomial basis and propagating toward the boundaries.

Figure 11 shows the variation of the L_∞ norm of the solution increments used as the convergence index to the steady-state solution for different orders of polynomial basis. As seen from this figure, the convergence index increases until the shock is formed at the center of the domain. The index then decreases showing a sign of convergence to the steady-state solution but finally stays nearly constant indicating the failure of the method to converge.

The problem is solved again with the same parameter defined earlier except for the number of collocation points. This time 101 equally distributed collocation points are used, 51 of which coinciding with the nodal points. Figure 12 shows the converged solutions of the problem for different polynomial basis of order zero, one and two, respectively. The best solution is obtained with basis of zero order that can be regarded as exact solution if small over and under shoots

DOI: 10.1002/fld

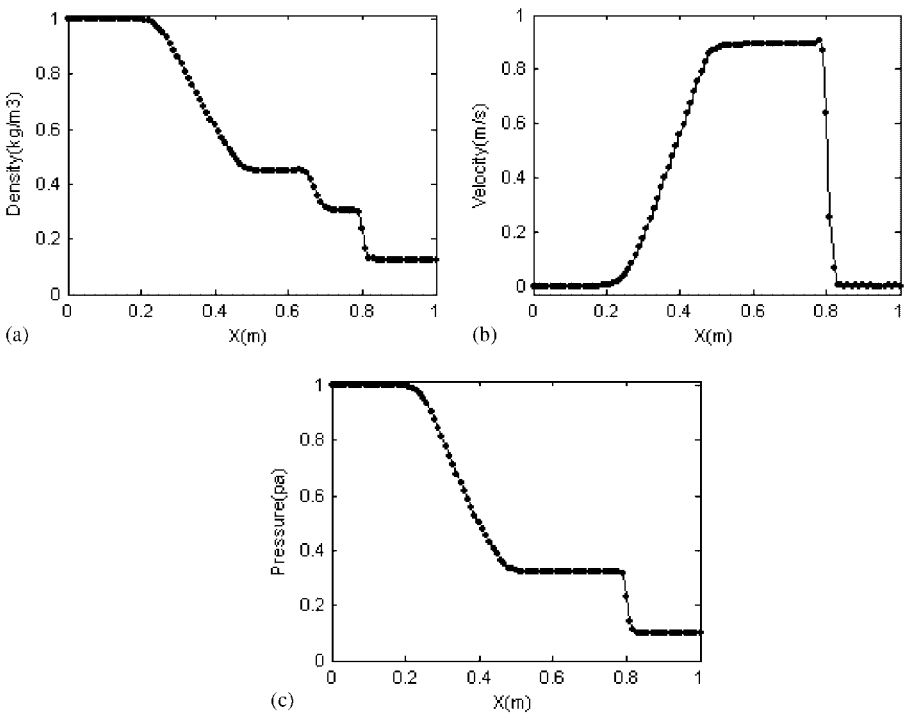

Figure 9. Variations of density (a), velocity (b) and pressure (c) obtained with $\theta = 0.7$ and 501 collocation points (shock tube).

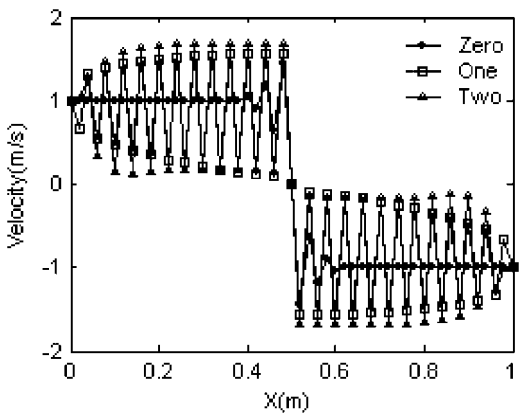

Figure 10. Un-converged solutions obtained using 51 collocation points at time 1 s (steady Burgers).

are neglected. It is seen that the oscillation of the numerical solution around the shock increases with the order of basis. This has been experienced with other numerical methods and in particular with the FEM in which the oscillation around high gradient solutions increases with the order

DOI: 10.1002/fld

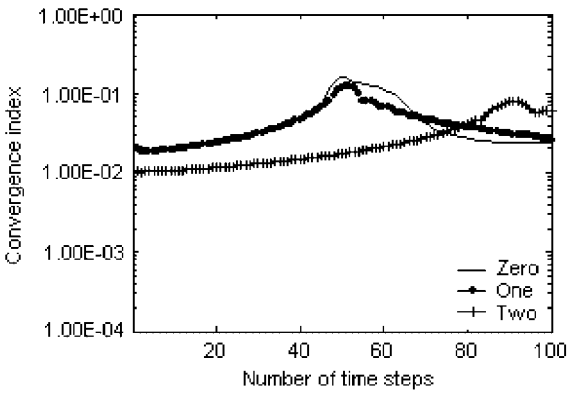

Figure 11. Convergence curves for different basis orders using 51 collocation points (steady Burgers).

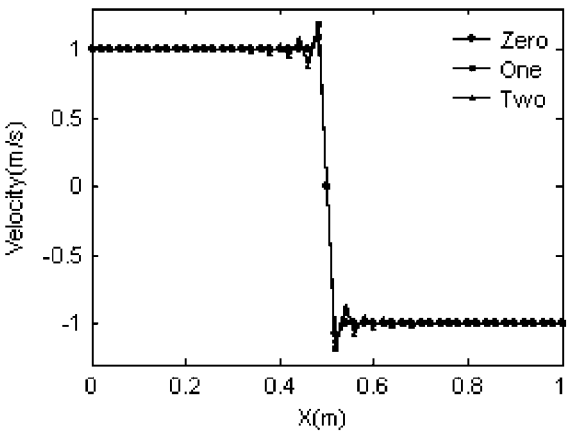

Figure 12. Steady solutions obtained using 101 collocation points (steady Burgers).

of interpolation used. Figure 13 shows the convergence curves of the method for different orders of the basis indicating that steady solution was obtained within only 66 time steps in all cases. Introduction of the extra collocation points seems to have played two major roles. First, the method is stabilized by suppressing the oscillations and subsequently producing nearly exact solution with lowest-order polynomial basis of zero. Second, the collocation points have improved the convergence characteristics of the method and hence have reduced the computational effort required to get the steady-state solution of the problem. This can be clearly seen by comparing the peaks of the two convergence curves corresponding to zero-order basis shown in Figures 11 and 13. These peaks indicate that the shock is formed at time step number 90 in the first run while this number is reduced to 45 when extra collocation points are used to construct the system of equations. With extra collocations, the method is in fact capable of producing the steady-state solution at time step 66 with much less computational effort than that required to form the shock in the first run.

DOI: 10.1002/fld

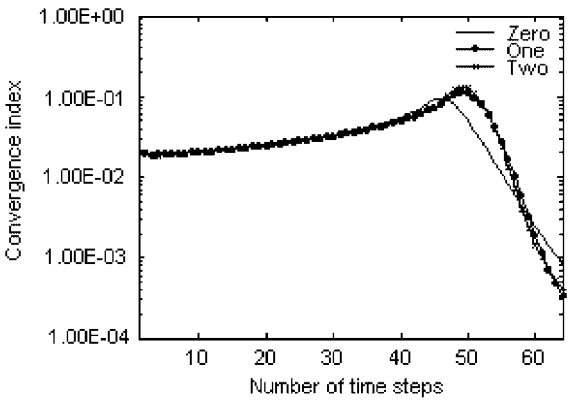

Figure 13. Convergence curves for different basis orders using 101 collocation points (steady Burgers).

4.5. Inviscid flow an ogee spillway

The flow of inviscid water over an ogee spillway is governed by the non-linear shallow-water equations in one dimension defined with the following parameters of Equation (16):

$$\mathbf{u}=\begin{bmatrix} H+\eta \\ (H+\eta)u \end{bmatrix}, \quad \mathbf{A}=\begin{bmatrix} 0 & 1 \\ -u^2+g(H+\eta) & 2u \end{bmatrix}, \quad \mathbf{Q}=\begin{bmatrix} 0 \\ g(H+\eta)\dfrac{\mathrm{d}H}{\mathrm{d}x} \end{bmatrix}$$

Here H is the flow depth, η is the surface elevation, u is the average velocity, $\underline{g}=9.81$ is the acceleration due to gravity and $\mathrm{d}H/\mathrm{d}x$ is the bed slope.

This problem is solved here on a mesh of 101 equally distributed nodes using a time step size of 0.4 s. The solution of the problem is again attempted for polynomial basis of zero, first and second order with radius of support domain equal to 0.3125, 0.3125 and 0.625 m, respectively. Numerical solution of the problem is first attempted using 101 collocation points coinciding with the nodal points. All the runs produced the same solution as shown in Figure 14.

The method, however, showed different convergence behavior for different polynomial basis used. Figure 15 shows the variation of the convergence index during the solution evolution for different polynomial basis. As shown in the figure, the method, though convergent for all basis, suffers from violent oscillation, which is represented by the highly oscillatory convergence curves. The method exhibits faster convergent behavior with polynomial basis order of 2 requiring about 70 time steps to reach the steady state.

To assess the effect of the collocation points, the problem was solved again with the same parameters defined earlier except for the number of collocation points. This time, 201 equally distributed collocation points are used, 101 of which coinciding with the nodal points. These runs produced the same solutions as those shown in Figure 15 due to the fact that the solution is smooth enough to be tackled by 101 collocation points, while showing different convergence characteristics. Figure 16 shows the convergence curves of these runs indicating smooth convergence of the method to the steady-state solution when extra collocations are used. Both first- and second-order bases were able to produce steady-state solution in only 45 time steps. Introduction of the

DOI: 10.1002/fld

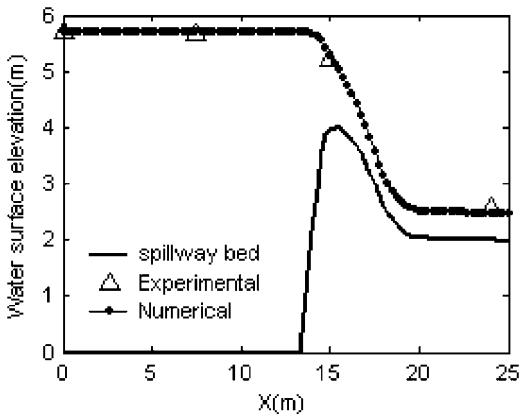

Figure 14. Steady water elevation over an ogee spillway.

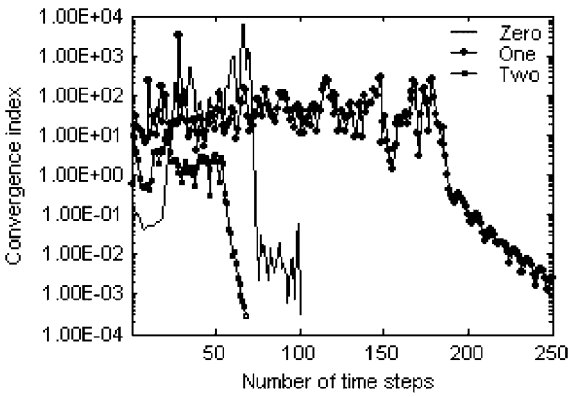

Figure 15. Convergence curves for different basis order using 101 collocation points (spillway flow).

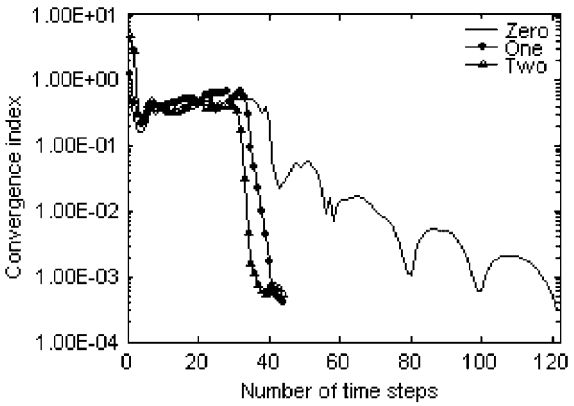

Figure 16. Convergence curves for different basis order using 201 collocation points (spillway flow).

DOI: 10.1002/fld

extra collocation points is clearly seen to have improved the efficiency of the method to get the steady-state solution.

4.6. Nozzle flow

In this section, simulation of steady-state compressible nozzle flow is performed by a time-marching algorithm. The governing equations in terms of the conservative variables are defined by the following parameters of Equation (16):

$$\mathbf{U}=\begin{bmatrix}\rho a\\ \rho a u\end{bmatrix},\quad \mathbf{A}=\begin{bmatrix}0 & 1\\ c^2-u^2 & 2u\end{bmatrix},\quad \mathbf{S}=\begin{bmatrix}0 & 0\\ \dfrac{c^2\,\mathrm{d}a}{a\,\mathrm{d}x} & 0\end{bmatrix}$$

Here ρ denotes the density, u is the velocity, c is the speed of sound (unity here), and a is the cross-sectional area of the nozzle. The cross-sectional area of the nozzle is described by the following equation:

$$a=1+\frac{(x-2.5)^2}{12.5},\quad 0\,\mathrm{m}<x<5\,\mathrm{m}$$

where x is the distance along the nozzle. The problem has an analytical solution defined as follows:

$$\rho a u=A_1$$

$$\frac{u^2}{2}+c^2 Ln(\rho)=A_2$$

where A_1 and A_2 can be determined by the boundary conditions. Under different inflow and outflow boundary conditions, three possible flow regimes can be expected:

(1) Subsonic inflow and subsonic outflow without shock.
(2) Subsonic inflow and supersonic outflow without shock.
(3) Subsonic inflow and subsonic outflow with a shock.

Case 1: *Subsonic inflow and subsonic outflow without shock*. In this case the flow remains subsonic throughout the nozzle. The variations of density along the nozzle is shown in Figure 17 and compared with the analytical solution using 41 collocation points coinciding with the nodal points. The time step size of $\Delta t=0.2\,\mathrm{s}$, $\theta=1$ and polynomial basis of order zero ($P=[1]$) are again employed in the computation. The result, though stable, suffers from some oscillations. The problem was solved again with 401 collocation points, 41 of which coinciding with the nodal points. Figure 18 illustrates the oscillation-free variation of density and velocity along the nozzle indicating the ability of collocation points to produce more accurate results. The same results are obtained using higher-order basis polynomials. Figures 19 and 20 show the variation of the convergence index for different polynomial orders of zero, one and two using 41 and 401 collocation points, respectively. It is seen that introduction of collocation points leads to exactly the same convergence characteristics of the method for different orders of the basis polynomial. In this case, collocation points do not improve the convergence characteristics of the method, perhaps due to smooth nature of the final solution.

Case 2: *Subsonic inflow and supersonic outflow without shock*. In this case, the subsonic flow is changed to supersonic flow at the sonic point ($u=c$) to conform to the exit boundary condition. The

DOI: 10.1002/fld

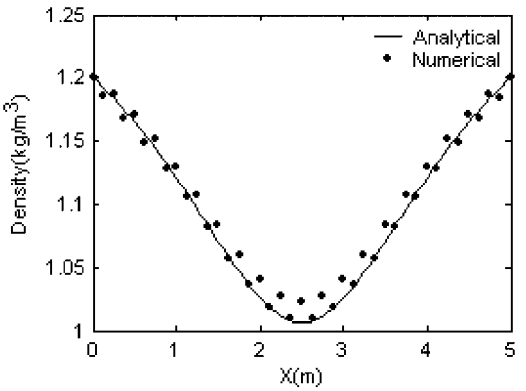

Figure 17. Numerical and analytical solutions for density using polynomial basis of order zero, and 41 collocation points (nozzle flow—case 1).

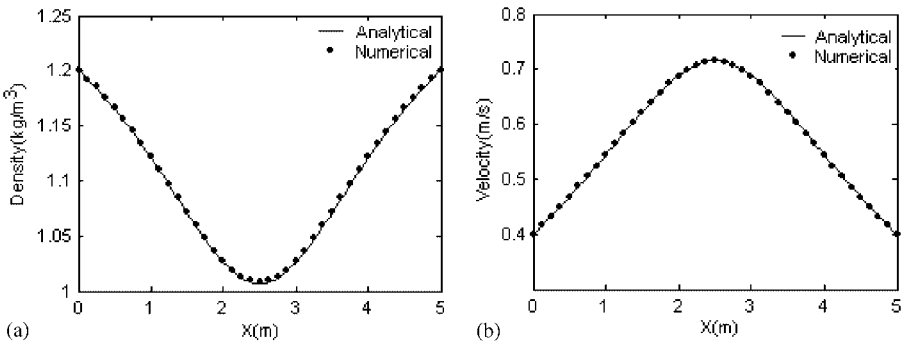

Figure 18. Numerical and analytical solutions for density (a) and velocity (b) using polynomial basis of order zero, and 401 collocation points (nozzle flow—case 1).

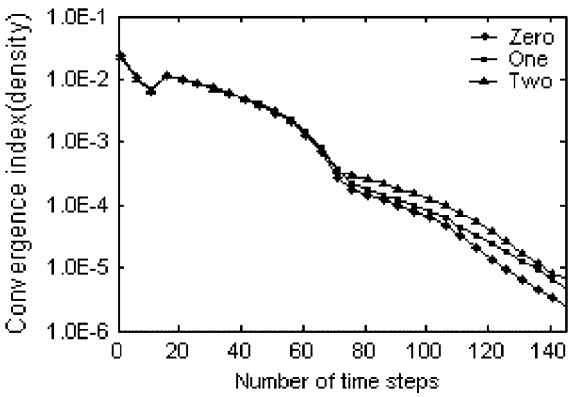

Figure 19. Convergence curves of density for different basis order using 41 collocation points (nozzle flow—case 1).

DOI: 10.1002/fld

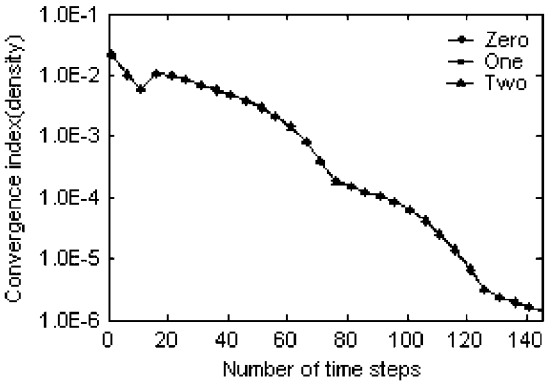

Figure 20. Convergence curves of density for different basis orders using 401 collocation points (nozzle flow—case 1).

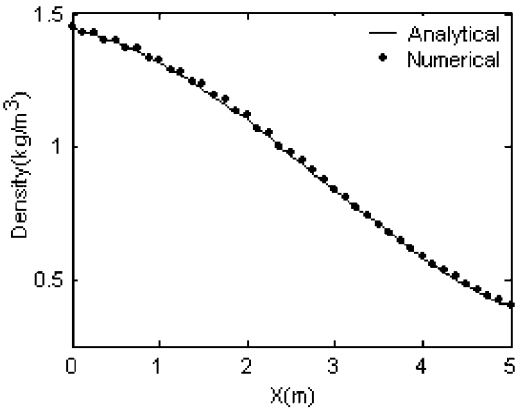

Figure 21. Numerical and analytical solution for density using polynomial basis of order zero, and 41 collocation points (nozzle flow—case 2).

computed density along the nozzle using the time step size of $\Delta t = 0.2$ s, polynomial basis of order zero ($P = [1]$) and 41 collocation points is compared with the analytical solution in Figure 21. The results show some minor oscillation especially for $x < 2$ m. The problem was solved again using 401 collocation points yielding the solutions shown in Figure 22 for density and velocity, respectively. It is again seen that introduction of extra collocation points leads to more stable and accurate solutions. Convergence curves of the method with and without extra collocation points shown in Figures 23 and 24 indicate that no improvement is again made in the convergence characteristics of the method by the introduction of collocation points.

Case 3: *Subsonic inflow and subsonic outflow with a shock*. In this case, the flow becomes supersonic after the sonic point. The flow then changes its regime from supersonic to subsonic via a shock before the downstream boundary to conform to the subsonic boundary condition. This problem is solved first with a time step size of $\Delta t = 0.25$ s, basis polynomial of $p = [1]$ and

DOI: 10.1002/fld

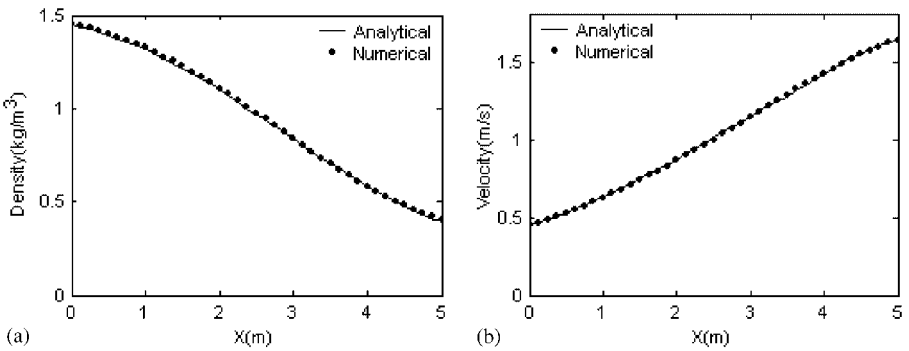

Figure 22. Numerical and analytical solution for density (a) and velocity (b) using polynomial basis of order zero, and 401 collocation points (nozzle flow—case 2).

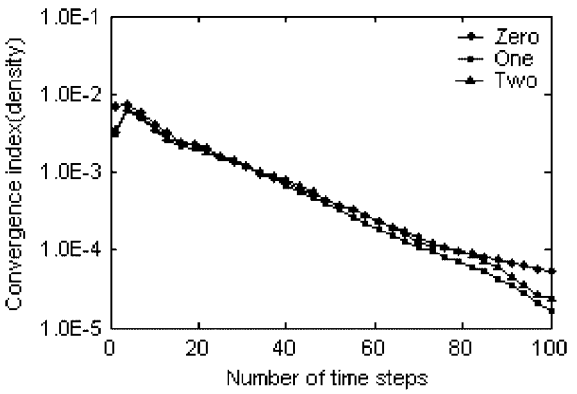

Figure 23. Convergence curves of density for different basis order using 41 collocation points (nozzle flow—case 2).

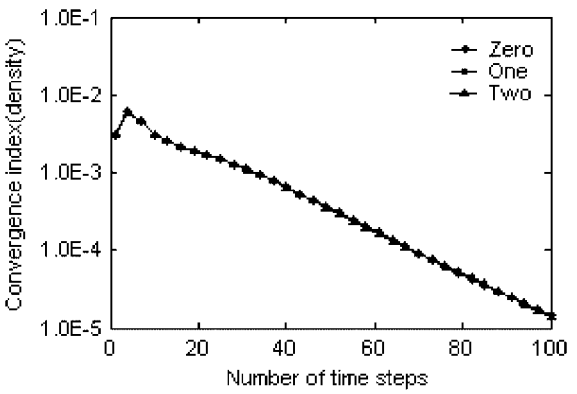

Figure 24. Convergence curves of density for different basis order using 401 collocation points (nozzle flow—case 2).

DOI: 10.1002/fld

101 collocation points coinciding with the 101 uniformly distributed nodal points. No converged solution could be obtained due to persistent oscillations at the shock position. The problem is solved again this time with 501 uniformly distributed collocation points, 101 of which coinciding with the nodal points. The variations of the computed density and velocity along the nozzle are compared in Figure 25 with those of the exact analytical solutions, respectively. These solutions are seen to be free of any oscillation. It is interesting to note that both the shock position and its strength are represented accurately for both of the variables. The same results were obtained using higher-order basis polynomials of order one and two, which are, therefore, not shown here. Finally Figure 26 illustrates the convergence characteristics of the method for different polynomial basis orders using 501 collocation points. The identical performance of the method for different basis orders can be contributed to the fact that linear interpolation between the boundary conditions used as the initial condition was not very far from the exact solution.

The ability of the proposed method in handling highly irregular meshes has already been demonstrated in [17] for one- and two-dimensional elliptic problems. Although it is natural to assume

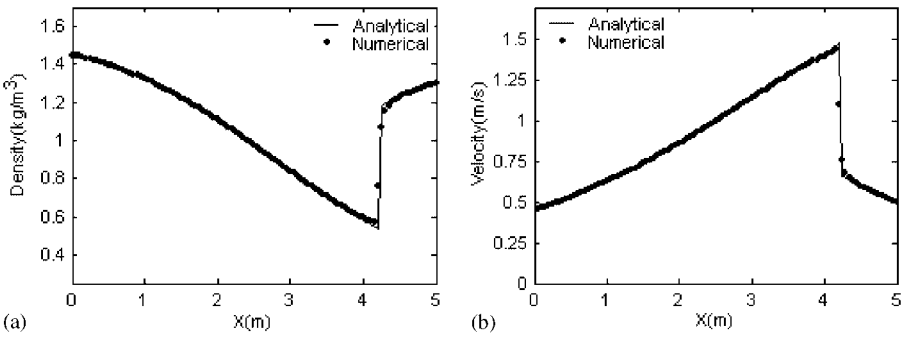

Figure 25. Numerical and analytical solution for density (a) and velocity (b) using polynomial basis of order zero, and 501 collocation points (nozzle flow—case 3).

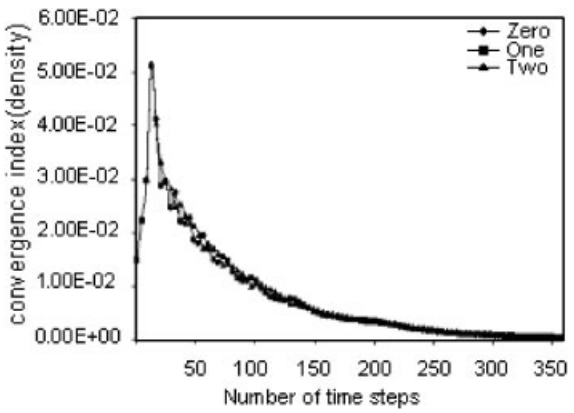

Figure 26. Convergence curves of density for different basis order using 501 collocation points (nozzle flow—case 3).

DOI: 10.1002/fld

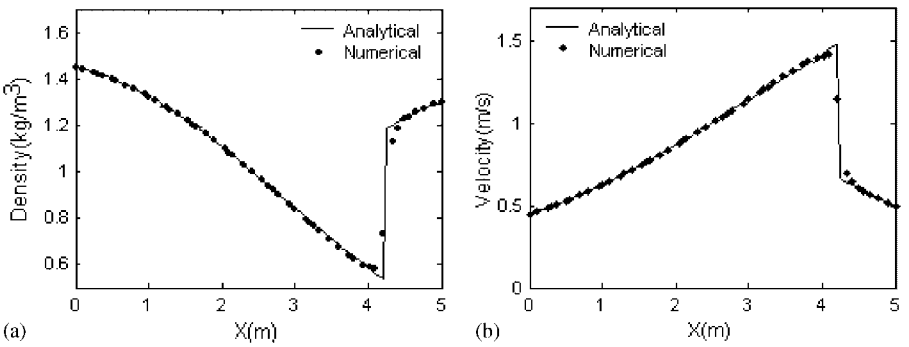

Figure 27. Numerical and analytical solution for density (a) and velocity (b) parameters on irregular mesh of nodes (nozzle flow—case 3).

that the method could preserve this ability for hyperbolic problems, the nozzle problem is solved on irregular mesh of nodes to emphasize on the ability of the method to handle non-uniform nodal positioning. Here the nozzle problem with the shocked solution (case 3) is chosen since it is more challenging than others. The problem is solved on an irregular mesh of 51 nodal points using the computational parameters of $\Delta t = 0.4\,\text{s}$, $P = [2]$, and radius of support domain equal to 0.15 m. A total of 501 collocation points are used, 51 of which coinciding with the nodal points and the rest uniformly distributed on the solution domain. Nodal distribution and the resulting numerical solutions for the velocity and density are presented and compared with the analytical solution in Figure 27. The figure clearly indicates the ability of the proposed method to represent the shocked solution in the case of irregular nodal distribution. This experiment was carried out with less number of nodal points so that the irregularity of the nodal distribution could be clearly illustrated.

5. CONCLUSION

In this paper a CDLSM method is introduced for the solution of transient and steady-state hyperbolic problems. The proposed method uses a fully least squares approach in both function approximation and discretization of the governing differential equations. The meshless shape functions were derived using the MLS method of function approximation. The method is based on minimization of a least squares functional defined as the weighted sum of the squared residual of the differential equation and its boundary condition at collocation points chosen on the domain and its boundaries. Although most of the existing meshless methods need background cells for numerical integration, the proposed method is truly meshless and does not require numerical integration procedure. The proposed method has additional advantages of producing symmetric, positive-definite matrices even for non-self-adjoint operators such as those encountered in fluid flow problems. Proposed method was used here to solve two sets of one-dimensional transient and steady-state hyperbolic benchmark problems, from both compressible and incompressible flow areas. The proposed method was shown to be a stable and accurate method for the solution of problems with shocked solutions. The collocation points were also shown not only to improve the accuracy of the results but also to contribute to the efficiency of the method when solving steady-state problems.

DOI: 10.1002/fld

REFERENCES

1. Belytschko T, Lu YY, Gu L. Element-free Galerkin methods. *International Journal for Numerical Methods in Engineering* 1994; **37**:229–256.
2. Nayroles B, Touzot G, Villon P. Generalizing the finite element method diffuse approximation and diffuse element. *Computational Mechanics* 1992; **10**:307–318.
3. Liu WK, Jun S, Zhang Y. Reproducing kernel particle methods. *International Journal for Numerical Methods in Engineering* 1995; **20**:1081–1106.
4. Gingold RA, Monaghan JJ. Smoothed particle hydrodynamics: theory and application to non-spherical stars. *Monthly Notices of the Royal Astronomical Society* 1977; **181**:375–389.
5. Ataie-Ashtiani B, Shobeyri G. Numerical simulation of landslide impulsive waves by incompressible smoothed particle hydrodynamics. *International Journal for Numerical Methods in Fluids* 2008; **56**(2):209–232.
6. Ataie-Ashtiani B, Farhadi L. A stable moving-particle semi-implicit method for free surface flows. *Fluid Dynamic Research* 2006; **38**(4):241–256.
7. Melenk JM, Babuska I. The partition of unity finite element method: basic theory and applications. *Computer Methods in Applied Mechanics and Engineering* 1999; **139**:289–314.
8. Atluri SN, Kim HG, Cho JY. A critical assessment of the truly meshless local Petrov–Galerkin (MLPG), and local boundary integral equation (LBIE) methods. *Computational Mechanics* 1999; **24**:348–372.
9. Onate E, Idelsohn S, Zienkiewicz OZ, Taylor RL. A finite point method in computational mechanics. Applications to convective transport and fluid flow. *International Journal for Numerical Methods in Engineering* 1996; **39**:3839–3867.
10. Zhang X, Liu XH, Song KZ, Lu MW. Least-squares collocation meshless method. *International Journal for Numerical Methods in Engineering* 2001; **51**:1089–1100.
11. Liu Y, Zhang X, Lu MW. A meshless method based on least-squares approach for steady and unsteady-state heat conduction problems. *Numerical Heat Transfer* 2005; **47**(Part B):257–275.
12. Liu X, Liu GR, Tai K, Lam KY. Radial basis point interpolation collocation method for 2-D solid problem. *The Second International Conference on Structural Stability and Dynamics*, Singapore, 16–18 December 2002.
13. Xiaofei P, Yim SK, Xiong Z. An assessment of the meshless weighted least-square method. *Acta Mechanica Solida Sinica* 2004; **17**(3):270–282.
14. Armentano MG, Durán RG. Error estimates for moving least square approximations. *Applied Numerical Mathematics* 2001; **37**:397–416.
15. Wang QX, Li H, Lam KY. Development of a new meshless-point weighted least-squares (PWLS) method for computational mechanics. *Computational Mechanics* 2005; **35**:170–181.
16. Afshar MH, Arzani H. Solving Poisson's equations by the discrete least square meshless method. *WIT Transactions on Modelling and Simulation* 2006; **42**:23–32.
17. Firoozjaee AR, Afshar MH. Discrete least squares meshless method with sampling points for the solution of elliptic partial differential equations. *Engineering Analysis with Boundary Elements* 2008; DOI: 10.1016/j.enganabound.2008.03.004.
18. Lancaster P, Salkauskas K. *Curve and Surface Fitting Introduction*. Academic Press: New York, 1986.
19. Liu GR, Gu YT. A local radial point interpolation method (LR-PIM) for free vibration analyses of 2-D solids. *Journal of Sound and Vibration* 2001; **246**(1):29–46.
20. Gu L. Moving kriging interpolation and element-free Galerkin method. *International Journal for Numerical Methods in Engineering* 2003; **56**:1–11.